

Can Artificial Noise Boost Further the Secrecy of Dual-hop RIS-aided Networks?

Elmehdi Illi, *Member, IEEE*, Marwa K. Qaraqe, *Senior Member, IEEE*, Faissal El Bouanani, *Senior Member, IEEE*, and Saif M. Al-Kuwari, *Senior Member, IEEE*

Abstract—In this paper, we quantify the physical layer security of a dual-hop regenerative relaying-based wireless communication system assisted by reconfigurable intelligent surfaces (RISs). In particular, the setup consists of a source node communicating with a destination node via a regenerative relay. In this setup, a RIS is installed in each hop to increase the source-relay and relay-destination communications reliability, where the RISs' phase shifts are subject to quantization errors. The legitimate transmission is performed under the presence of a malicious eavesdropper attempting to compromise the legitimate transmissions by overhearing the broadcasted signal from the relay. To overcome this problem, we incorporate a jammer to increase the system's secrecy by disrupting the eavesdropper through a broadcasted jamming signal. Leveraging the well-adopted Gamma and Exponential distributions approximations, the system's secrecy level is quantified by deriving approximate and asymptotic expressions of the secrecy intercept probability (IP) metric in terms of the main network parameters. The results show that the secrecy is enhanced significantly by increasing the jamming power and/or the number of reflective elements (REs). In particular, an IP of approximately 10^{-4} can be reached with 40 REs and 10 dB of jamming power-to-noise ratio even when the legitimate links' average signal-to-noise ratios are 10-dB less than the eavesdropper's one. We show that cooperative jamming is very helpful in strong eavesdropping scenarios with a fixed number of REs, and the number of quantization bits does not influence the secrecy when exceeding 3 bits. All the analytical results are endorsed by Monte Carlo simulations.

Index Terms—Cooperative jamming, decode-and-forward, intercept probability, phase quantization errors, reconfigurable intelligent surfaces.

I. INTRODUCTION

The past few decades witnessed significant efforts on designing ultra-reliable, self-sustainable, and secure communications, pillars representing the main targets of the 5G and beyond and 6G visions [2], [3]. In fact, information security has always been a *de facto* concern in wireless transmissions due to their broadcast nature [4]. To date, the implementation of security mechanisms on wireless communication systems (WCSs) has been viewed almost exclusively from higher layers by grasping the key-based cryptographic algorithms [4]. However, while these algorithms provide the required security

for devices with sufficient transmit power and computing facilities onboard [5], the emergence of new wireless paradigms, such as the internet of things (IoT) and vehicular communications renders current cryptographic schemes unsuited for such power-limited and processing-restricted technologies [6]. Furthermore, the forecasted sizeable amount of data traffic is expected to bring unprecedented privacy leakages [7].

Recently, physical layer security (PLS) has been gaining significant attention from both academia and industry communities. Unlike the conventional key-based cryptographic schemes, PLS establishes secure transmissions leveraging exclusively the physical layer parameters (e.g., fading, channel coding, interference, etc) [8], [9] in order to provide a noisy legitimate signal copy to the eavesdropper (i.e., increasing its equivocation). The secrecy capacity is PLS's cornerstone, for which higher values correspond to an improved system's security level from the physical layer point of view. To this end, PLS can effectively contribute to providing acceptable security levels with a much-reduced overhead in comparison with the traditional cryptographic schemes [5].

Regular WCSs consist of a transmitter sending an information-bearing signal to a receiver through an uncontrollable propagation medium. This signal reaches the destination via several replicas through multiple reflection paths, producing random fading [10]. However, futuristic wireless networks such as the 6G are envisioned to adopt the *Smart Radio Environment*, where every network component can adapt to the changes in the environment [11]. To this end, considerable attention has been paid in the yesteryears to the *Reconfigurable Intelligent Surface* (RIS) technology as a key enabler to spectrum and energy efficiency's boosting [12]. A RIS is a man-made metasurface consisting of a large number of low-cost passive reflecting elements (REs), where each of which can tune its phase shift to adapt to the incident electromagnetic wave impinging its surface. As a result, such reflected signal copies can be constructively/destructively superposed at the intended/unintended node to maximize/minimize the received signal power; a process that resembles the well-known MIMO beamforming [13].

The inherent capabilities of RISs and metasurfaces in reshaping the propagation environment have driven intuitive insights into exploiting these features in favor of boosting the system's secrecy. As illegitimate network users can benefit from different signal qualities, which poses serious eavesdropping threats, RIS can be used to effectively choose optimal phase shifts in favor of the legitimate user; i.e., beamsteer the

This paper was submitted in part to BalkanCom 2022 [1].

This research was sponsored in part by the NATO Science for Peace and Security Programme under grant SPS G5797.

E. Illi, M. K. Qaraqe, and S. M. Al-Kuwari are with the College of Science and Engineering, Hamad Bin Khalifa University, Qatar Foundation, Doha, Qatar. (e-mails: elmehdi.illi@ieee.org, {mqaraqe, smalkuwari}@hbku.edu.qa).

F. El Bouanani is with ENSIAS College of Engineering, Mohammed V University of Rabat, Morocco. (e-mail: f.elbouanani@um5s.net.ma).

information signal to the genuine user with a higher power, while providing the eavesdropper with a lower signal power.

A. Related Work

The corresponding literature of related work involving PLS and RIS has done a substantial contribution to the subject so far. In particular, the authors in [14] consider the PLS of a two-way multi-user RIS-assisted transmission for which a user scheduling scheme was proposed. In [15], the secrecy level of a RIS-assisted WCS was tackled where a direct link between the transmitter and the receiver was considered. In [16], the authors carried out a PLS analysis of a RIS-based two-users non-orthogonal multiple access network. Similarly, the work in [17] inspected the security performance of a RIS-aided network with an uncertain eavesdropper location. Moreover, several work dealt with the secrecy maximization problem by optimizing the RIS and system parameters. For instance, the authors in [18] formulated a secrecy rate-maximization problem under the RIS-assisted system constraints and proposed an efficient algorithm for solving the optimization problem. Similarly, an energy-efficiency secure transmission problem for a multi-antenna source RIS-assisted multi-user network was formulated in [19] with the probabilistic outage constraint. In addition, the authors in [20] formulated a secrecy-rate maximization problem of a non-orthogonal unicast-multicast network, where alternate optimization-based solutions were adopted for optimizing the non-orthogonal power splitting and RIS's phase shifts. M. H. Khosafa *et al.* inspected the secrecy performance of a RIS-assisted device-to-device WCS subject to interference from another cellular user [21]. Also, a comprehensive secrecy analysis for similar RIS-assisted WCSs in distinct setups was carried out in other work such as [13], [14], [22] and references therein.

B. Motivation

Although the aforementioned work brought interesting contributions on the PLS analysis and optimization of RIS-aided WCSs, they were constrained by the assumption of error-free phase shift estimation and quantization. In fact, reaching a high-precision configuration for the RIS is impractical [23]. The authors in [23] provided a bit error probability analysis of a RIS-assisted system subject to phase estimation and quantization errors. Importantly, Sánchez *et al.* assessed the secrecy performance analysis of a RIS-based network subject to the presence of phase estimation and quantization errors [24]. Furthermore, the work in [25], [26] extended the secrecy analysis of such a WCS by considering phase estimation and quantization errors along with multiple eavesdroppers under the presence and absence of a direct link, respectively. On the other hand, a limited number of work in the literature analyzed the interplay between conventional dual/multi-hop relaying techniques and RIS when incorporated together on a transmission system. Differently from the RIS principle, relaying techniques actively process the signal by either amplifying it (amplify-and-forward (AF)), or decoding it (decode-and-forward (DF)), before handing it to the next relay or destination node. To this end, work such as [27]–[29] aimed to amalgamate the benefits of both RIS and active relaying schemes

on the PLS. In [27], the authors assessed the PLS analysis of a three-hop mixed visible light communication/radio-frequency (RF) WCS whereby a RIS is used to assist the second hop (i.e., RF channel). Furthermore, the authors of [28] aimed at optimizing both RIS phase shifts and relay selection in a multi-relay dual-hop network through deep reinforcement learning, where a RIS was involved to assist both hops. The secrecy level of a mixed RF-underwater optical WCS was quantified in [29] with a single RIS assisting the first RF hop, under the presence of a single eavesdropper.

Combining RIS and cooperative relaying schemes has been appealing in a multi-hop scenario; e.g., wireless mesh network [30]; where the different relaying transceivers can be located in a non-line-of-sight environment. This motivates the implementation of numerous RISs to accommodate reliable transmissions. On the other hand, the inclusion of cooperative jamming/artificial noise has been shown to provide significant improvement in system secrecy. Importantly, several works such as [21], [31] analyzed and discussed the interplay between RIS and jamming schemes in enhancing the PLS of WCSs. Therefore, it is crucial to provide a comprehensive PLS analysis of dual-hop relay-based networks assisted by RIS along with jamming, by considering phase estimation and/or quantization errors.

C. Contributions

Motivated by the above, we aim in this paper at analyzing the secrecy performance of a dual-hop RIS and jamming-aided WCS. Particularly, two multi-element RISs are involved to assist the transmission of each of the two hops, i.e. source-relay and relay-destination, where the DF relaying scheme is implemented at the relay. In addition to this, a malicious eavesdropper is attempting to overhear the signal broadcasted by the relay and reflected by the second RIS. Additionally, a jammer is incorporated to deceive the eavesdropper by injecting a jamming signal, assumed to be canceled perfectly at the legitimate destination. Lastly, the RIS-assisted transmission is assumed to be subject to phase quantization errors (PQEs). The current work differs from [24]–[29] where the PLS analysis was carried out by considering either perfect phase estimation and quantization or dual-hop relaying, while the involvement of cooperative jamming was not considered. To the best of our knowledge, the current work is the first of its kind to inspect the joint influence of the DF relaying scheme and cooperative jamming along with RIS affected by PQEs on the PLS. In detail, the main contributions of this work can be summarized as follows:

- By virtue of the well-adopted Gamma and Exponential distributions as accurate approximations, we provide an approximate expression for the system's intercept probability (IP) metric in terms of key setup parameters, such as the per RIS number of REs, jamming-to-noise power ratio, legitimate and eavesdropper's links' average signal-to-noise ratios (SNRs), and the number of quantization bits.
- We derive an asymptotic expression for the IP in the high SNR regime, whereby the underlying coding gain and

Symbol	Meaning	Symbol	Meaning
S	Source	η_i	$L^{(2)}$'s i th element phase shift
R	Relay	$\xi_i^{(l)}$	$L^{(l)}$'s i th element PQE
D	Destination	$F^{(c)}(\cdot)$	Complementary cumulative distribution function
J	Jammer	$\Gamma_{\text{inc}}(\cdot, \cdot)$	Upper-incomplete Gamma function
E	Eavesdropper	$\Gamma(\cdot)$	Gamma function
$L^{(l)}$	l -th RIS ($l = 1, 2$)	m_{UV}	Gamma distribution's shape parameter for the U - V link
M	$L^{(1)}$'s number of REs	Ω_{UV}	Average equivalent fading power for the U - V link
N	$L^{(2)}$'s number of REs	$(\varphi_{l,k})_{l=1,2}$	k th moment of the PQEs of $L^{(l)}$
γ_{UV}	U - V link's path-loss-normalized instantaneous SNR/SINR	$(n_{b_l})_l$	$L^{(l)}$'s number of quantization bits
$\bar{\gamma}_{UV}$	U - V link's path-loss-normalized average SNR	$\mathbb{E}[\cdot]$	Expected value
P_U	Transmit power of node U	$f(\cdot)$	Probability density function
σ_V^2	Additive white Gaussian noise power at V	$F(\cdot)$	Cumulative distribution function
h_{XY}	XY link's complex-valued fading coefficient	C_s	Secrecy capacity
$\mathcal{CN}(\mu, \sigma^2)$	Complex Gaussian distribution of mean μ and variance σ^2	P_{int}	Intercept probability
ϕ_i	$L^{(1)}$'s i th element phase shift	$H_{\cdot, \cdot, \cdot, \cdot}(\cdot, \cdot \cdot)$	Bivariate Fox's H -function

TABLE I: List of symbols.

diversity order are quantified. The results show that the secrecy diversity order is proportional to the minimum of the two RISs' number of REs.

- We show analytically that the system's secrecy level improves by increasing the number of REs and/or number of quantization bits. In addition to this, we prove that the SNRs of the legitimate and wiretap links are uncorrelated although they share some common terms.
- We provide extensive numerical and simulation results in order to quantify the secrecy level of the system versus the various parameters involved. We found that an IP around 10^{-4} can be reached with 40 REs per RIS and 10 dB of jamming power-to-noise ratio even when the legitimate links' average SNRs are 10 dB below the eavesdropper's one.

D. Organization

The rest of this paper is structured as follows: In Section II, the adopted system model is detailed, while in Section III, we provide some statistics of the different channels' SNRs. In Section IV, we derive approximate and high-SNR asymptotic expressions for the IP and provide several analytical insights and discussions on the influence of some key system parameters on the system's security. Numerical and simulation results are presented and discussed in Section V. Finally, Section VI concludes the paper.

E. Notations

Table I lists the symbols and notations used in this paper.

II. SYSTEM MODEL

We consider a dual-hop RIS-assisted wireless network as depicted in Fig. 1, where a source node (S) communicates with a destination node (D) with the help of a DF-based relay (R). Additionally, two RISs, $L^{(1)}$ and $L^{(2)}$, with M and N REs, respectively, are installed to assist the S - R and R - D transmissions. Furthermore, an eavesdropper (E) attempts to compromise the legitimate link by overhearing the signal broadcasted by R . Moreover, a jammer (J) enhances the

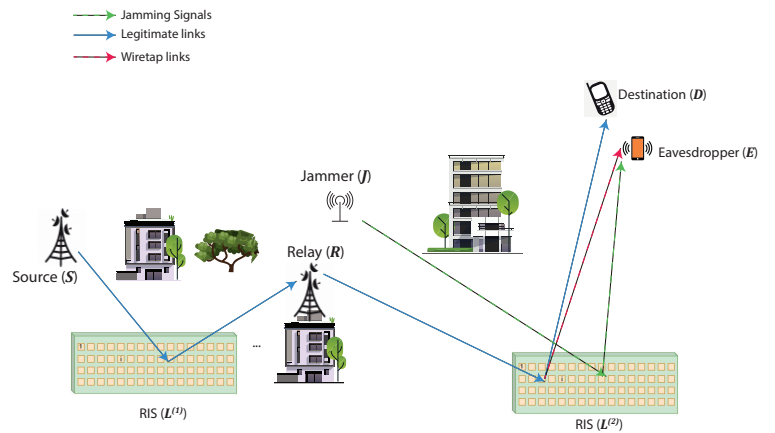


Fig. 1: System model.

communication's security level by broadcasting a jamming signal to disrupt E ; assuming that D is able to remove such a jamming signal through some artificial noise cancellation mechanism [32]. Due to the long distance between the nodes, the direct-link signals of the S - R , R - D , R - E , S - E , J - E , and S - D channels can be neglected. Lastly, it is assumed that all the nodes in the network are equipped with a single antenna.

The received per-hop SNRs at D and R are given as

$$\gamma_{SR} = \bar{\gamma}_{SR} \left| \sum_{i=1}^M h_{SL_i^{(1)}} h_{L_i^{(1)}R} \exp(j\phi_i) \right|^2, \quad (1)$$

$$\gamma_{RD} = \bar{\gamma}_{RD} \left| \sum_{i=1}^N h_{RL_i^{(2)}} h_{L_i^{(2)}D} \exp(j\eta_i) \right|^2, \quad (2)$$

respectively, where $\bar{\gamma}_{UV} = \frac{P_U}{\sigma_V^2}$ is the path-loss-normalized average SNR of the U - V link with $UV \in \{SR, RD\}$, P_U is the transmit power of node U , σ_R^2 and σ_D^2 are the respective additive white Gaussian noise powers at R and D , respectively, $h_{SL_i^{(1)}}$, $h_{L_i^{(1)}R}$, $h_{RL_i^{(2)}}$, and $h_{L_i^{(2)}D}$ are the channel fading coefficients of the S - $L_i^{(1)}$, $L_i^{(1)}$ - R , R - $L_i^{(2)}$ and $L_i^{(2)}$ - D links, respectively, assumed to be independent and identically distributed zero-mean complex Gaussian random variables (RVs)

with distribution $\mathcal{CN}(0, 1)$, i.e., Rayleigh fading, where $L_i^{(l)}$ ($l = 1, 2$) is $L^{(l)}$'s i th RE, $j = \sqrt{-1}$, and ϕ_i and η_i are the phase shifts of $L^{(1)}$ and $L^{(2)}$'s i th RE, respectively. On the other hand, the instantaneous signal-to-interference-and-noise ratio (SINR) at E can be written as

$$\gamma_{RE} = \frac{\bar{\gamma}_{RE} \left| \sum_{i=1}^N h_{RL_i^{(2)}} h_{L_i^{(2)}E} \exp(j\eta_i) \right|^2}{\bar{\gamma}_{JE} \left| \sum_{i=1}^N h_{JL_i^{(2)}} h_{L_i^{(2)}E} \exp(j\eta_i) \right|^2 + 1}, \quad (3)$$

where $h_{JL_i^{(2)}}$ is the fading coefficient of the J - $L_i^{(2)}$ link.

Furthermore, we assume a perfect channel state information (CSI) estimation at the two RISs¹, while the estimated phase is subject to quantization errors. To this end, the phase shifts of the i -th element of $L^{(l)}$ ($l = 1, 2$) are given by [23]

$$\phi_i = - \left[\arg \left(h_{SL_i^{(1)}} \right) + \arg \left(h_{L_i^{(1)}R} \right) \right] + \xi_i^{(1)}, 1 \leq i \leq M \quad (4)$$

and

$$\eta_i = - \left[\arg \left(h_{RL_i^{(2)}} \right) + \arg \left(h_{L_i^{(2)}D} \right) \right] + \xi_i^{(2)}, 1 \leq i \leq N, \quad (5)$$

respectively, where $\xi_i^{(l)}$ are the corresponding PQE at the i -th elements of $L^{(l)}$ ($l = 1, 2$). As a result, the corresponding per-hop SNRs at R and D and the SINR at E , given by (1), (2), and (3), respectively, become

$$\gamma_{SR} = \bar{\gamma}_{SR} \left| \sum_{i=1}^M \left| h_{SL_i^{(1)}} \right| \left| h_{L_i^{(1)}R} \right| \exp \left(j\xi_i^{(1)} \right) \right|^2, \quad (6)$$

$$\gamma_{RD} = \bar{\gamma}_{RD} \left| \sum_{i=1}^N \left| h_{RL_i^{(2)}} \right| \left| h_{L_i^{(2)}D} \right| \exp \left(j\xi_i^{(2)} \right) \right|^2, \quad (7)$$

and

$$\gamma_{RE} = \frac{\underbrace{\bar{\gamma}_{RE} \left| \sum_{i=1}^N \left| h_{RL_i^{(2)}} \right| \left| h_{L_i^{(2)}E} \right| \exp(j\varpi_i) \right|^2}_{\triangleq \Gamma_{RE}}}{\underbrace{\bar{\gamma}_{JE} \left| \sum_{i=1}^N h_{JL_i^{(2)}} h_{L_i^{(2)}E} \exp(j\eta_i) \right|^2}_{\triangleq \Gamma_{JE}} + 1}, \quad (8)$$

with

$$\varpi_i = \arg \left(h_{L_i^{(2)}E} \right) - \arg \left(h_{L_i^{(2)}D} \right) + \xi_i^{(2)}. \quad (9)$$

III. STATISTICAL PROPERTIES

The legitimate instantaneous SNR expressions in (6) and (7) are incorporating the residual PQEs of $L^{(1)}$ and $L^{(2)}$, respectively. For a given number of quantization bits, such SNRs can be accurately approximated by a Gamma distribution

¹The end-to-end legitimate channels estimation (S - $L^{(1)}$ - R and R - $L^{(2)}$ - D) is performed at R and D , respectively, by sending pilot symbols from S and R over various RIS phase configurations, whereby the cascaded channel can be estimated linearly by combining the corresponding received signals. Afterward, the channel coefficients are fed back to the RISs' controllers, by which appropriate phase shifts can be selected accordingly [33].

where the approximate complementary cumulative distribution function (CCDF) can be derived by virtue of integrating the probability density function (PDF) in [23, Eq. (13)] as follows

$$F_{\gamma_{UV}}^{(c)}(z) \approx \frac{\Gamma_{\text{inc}} \left(m_{UV}, \frac{m_{UV}}{\Omega_{UV} \bar{\gamma}_{UV}} z \right)}{\Gamma(m_{UV})}, UV \in \{SR, RD\}, \quad (10)$$

with $\Gamma_{\text{inc}}(\cdot, \cdot)$ and $\Gamma(\cdot)$ are the upper-incomplete and complete Gamma functions, respectively [34, Eqs (8.350.2, 8.310.1)]. Furthermore, by considering the Rayleigh fading model²

over all channels, we have $m_{UV} = \frac{\mathcal{K}}{2} \frac{\varphi_{l,1}^2 \frac{\pi^2}{16}}{1 + \varphi_{l,2} - 2\varphi_{l,1}^2 \frac{\pi^2}{16}}$, $\mathcal{K} = \begin{cases} M, & \text{if } UV = SR \\ N, & \text{if } UV = RD \end{cases}$, $l = \begin{cases} 1, & \text{if } UV = SR \\ 2, & \text{if } UV = RD \end{cases}$, $\varphi_{l,k} = \mathbb{E} \left[\exp \left(jk\xi_i^{(l)} \right) \right]$, and $\Omega_{UV} = \left(\frac{\mathcal{K}\pi\varphi_{l,1}}{4} \right)^2$ [23]. When only a finite set of $2^{n_{b_l}}$ phases can be configured at the l th RIS, with n_{b_l} being the corresponding number of quantization bits, the PQE $\xi_i^{(l)}$ is uniformly distributed over the interval $\left[-\frac{\pi}{2^{n_{b_l}}}, \frac{\pi}{2^{n_{b_l}}} \right]$ with $\varphi_{l,k} = \frac{2^{n_{b_l}+1-k} \sin(2^{k-1-n_{b_l}}\pi)}{\pi}$ [23].

Remark 1. The per-hop SNRs (γ_{SR} and γ_{RD}) are approximated by Gamma-distributed RVs with shape parameter

$$m_{UV} = \frac{\mathcal{K}}{2} \frac{\varphi_{l,1}^2 \frac{\pi^2}{16}}{1 + \varphi_{l,2} - 2\varphi_{l,1}^2 \frac{\pi^2}{16}}, UV \in \{SR, RD\}, \quad (11)$$

and scale parameter $\frac{\Omega_{UV} \bar{\gamma}_{UV}}{m_{UV}}$ with

$$\Omega_{UV} = \frac{\mathcal{K}^2}{16} \left(\frac{\pi \sin(X)}{X} \right)^2, X \in \left[0, \frac{\pi}{2} \right], \quad (12)$$

where $X = \frac{\pi}{2^{n_{b_l}}}$ and $n_{b_l} \in [1, \infty[$. On the other hand, the average value of γ_{UV} is the product of its shape and scale parameters, i.e.,

$$\mathbb{E}[\gamma_{UV}] = \Omega_{UV} \bar{\gamma}_{UV}, \quad (13)$$

which is proportional to Ω_{UV} .

1) By differentiating Ω_{UV} with respect to X , one obtains

$$\frac{\partial \Omega_{UV}}{\partial X} = \frac{\mathcal{K}^2 \pi^2 \sin(X) \cos(X)}{8X^3} (X - \tan(X)). \quad (14)$$

As $\sin(X) \geq 0$ and $\cos(X) \geq 0$ for $X \in [0, \frac{\pi}{2}]$, the above derivative's sign depends on the one of $g(X) = X - \tan(X)$. To this end, we have the following

$$g'(X) = 1 - \sec^2(X), \quad (15)$$

where $\sec(\cdot) = \frac{1}{\cos(\cdot)}$ is the secant function, which is obviously greater than or equal to 1 for $X \in [0, \frac{\pi}{2}]$. Hence, $g'(X) \leq 0$ over this latter interval which yields that (i) $g(X)$ is a decreasing function over the same interval. Furthermore, we have (ii)

$$\lim_{x \rightarrow 0} g(X) = 0, \quad (16)$$

$$\lim_{x \rightarrow \frac{\pi}{2}} g(X) = -\infty. \quad (17)$$

²The channel between the various nodes and the RIS elements can be represented by the Rayleigh fading model, as was considered in various studies such as [15], [16], [35], [36]. Such a model can be used in the considered case of the absence of a line-of-sight link between the nodes and the RIS.

Thus, leveraging (i) and (ii), $g(X) \leq 0$ for $X \in [0, \frac{\pi}{2}]$. Therefore, Ω_{UV} is a decreasing function of X . On the other hand, it is obvious that X is inversely proportional to n_{bi} . As a result, Ω_{UV} is increasing in terms of n_{bi} . Thus, the higher the number of quantization bits, the greater Ω_{UV} , leading to higher average value of the per-hop legitimate SNR, i.e., $\mathbb{E}[\gamma_{UV}]$.

2) We can infer from (12) and (13) that the average legitimate SNRs, i.e., $\mathbb{E}[\gamma_{SR}]$ and $\mathbb{E}[\gamma_{RD}]$, scale with M^2 and N^2 , respectively. Therefore, the higher the number of REs, the greater the legitimate per hop SNRs.

Since R performs DF relaying protocol, the end-to-end (e2e) SNR can be written as [9, Eq. (13)]

$$\gamma_{eq} = \min(\gamma_{SR}, \gamma_{RD}), \quad (18)$$

where the underlying CCDF is given as

$$F_{\gamma_{eq}}^{(c)}(x) = F_{\gamma_{SR}}^{(c)}(x) F_{\gamma_{RD}}^{(c)}(x). \quad (19)$$

It has been demonstrated in [23], [24] that the random variables (RVs) Γ_{RE} and Γ_{JE} , given in the numerator and denominator of (8), respectively, can be approximated by an Exponential distribution with PDF and cumulative distribution function (CDF) expressed as

$$f_{\Gamma_{UE}}(z) \approx \frac{1}{N\bar{\gamma}_{UE}} \exp\left(-\frac{z}{N\bar{\gamma}_{UE}}\right), U \in \{R, J\} \quad (20)$$

and

$$F_{\Gamma_{UE}}(z) \approx 1 - \exp\left(-\frac{z}{N\bar{\gamma}_{UE}}\right), U \in \{R, J\}, \quad (21)$$

respectively, with an average value of

$$\mathbb{E}[\Gamma_{UE}] = N\bar{\gamma}_{UE}, U \in \{R, J\}. \quad (22)$$

As a consequence, the CDF of γ_{RE} , defined by (8), can be computed as follows

$$F_{\gamma_{RE}}(z) \triangleq \int_0^\infty F_{\Gamma_{RE}}(z(x+1)) f_{\Gamma_{JE}}(x) dx \quad (23)$$

$$\stackrel{(a)}{\approx} \frac{1}{N\bar{\gamma}_{JE}} \int_0^\infty \left(1 - \exp\left(-\frac{z(x+1)}{N\bar{\gamma}_{RE}}\right)\right) \times \exp\left(-\frac{x}{N\bar{\gamma}_{JE}}\right) dx, \quad (24)$$

$$\stackrel{(b)}{=} 1 - \frac{\exp\left(-\frac{z}{N\bar{\gamma}_{SE}}\right)}{\frac{\bar{\gamma}_{JE}}{\bar{\gamma}_{SE}}z + 1}. \quad (25)$$

By incorporating (20) with $U = J$ and (21) with $U = R$ into (23), Step (a) is reached, while Step (b) is formed relying on the change of variable $t = x + 1$ and the integral of the exponential function.

Consequently, the respective PDF is readily obtained by a differentiation of (25) with respect to z as

$$f_{\gamma_{RE}}(z) \approx \frac{\exp\left(-\frac{z}{N\bar{\gamma}_{RE}}\right) [\bar{\gamma}_{JE}N\bar{\gamma}_{RE} + \bar{\gamma}_{RE} + \bar{\gamma}_{JE}z]}{N(\bar{\gamma}_{RE} + \bar{\gamma}_{JE}z)^2}. \quad (26)$$

Remark 2. Leveraging (22), the average value of the eavesdropper link's SINR (i.e., γ_{RE}), given by (8), can be written as

$$\begin{aligned} \mathbb{E}[\gamma_{RE}] &= \frac{\mathbb{E}[\Gamma_{RE}]}{\mathbb{E}[\Gamma_{JE}] + 1} \\ &= \frac{N\bar{\gamma}_{RE}}{N\bar{\gamma}_{JE} + 1}. \end{aligned} \quad (27)$$

Importantly, in the absence of jamming (i.e., $\bar{\gamma}_{JE} = 0$), which is among optimal scenarios for the eavesdropper, one obtains $\mathbb{E}[\gamma_{RE}] = N\bar{\gamma}_{RE}$, which scales with N . On the other hand, when $\bar{\gamma}_{RE} = \bar{\gamma}_{JE} \rightarrow \infty$, one obtains $\mathbb{E}[\gamma_{RE}] = 1$, which scales independently of N .

Lemma 1 (Independence of the Relay-Destination, Jammer-Eavesdropper, and Relay-Eavesdropper's Cascaded Fading). *The cascaded fading coefficients of the legitimate second hop, eavesdropper, and jammer-eavesdropper links, given by*

$$g_{RD} = \sum_{i=1}^N \left| h_{RL_i^{(2)}} \right| \left| h_{L_i^{(2)}D} \right| \exp\left(j\xi_i^{(2)}\right), \quad (28)$$

$$g_{RE} = \sum_{i=1}^N \left| h_{RL_i^{(2)}} \right| \left| h_{L_i^{(2)}E} \right| \exp(j\varpi_i), \quad (29)$$

and

$$g_{JE} = \sum_{i=1}^N h_{JL_i^{(2)}} h_{L_i^{(2)}E} \exp(j\eta_i), \quad (30)$$

respectively, are mutually independent.

Proof: The proof is provided in Appendix A. ■

IV. PHY SECURITY ANALYSIS

In this section, novel approximate and high-SNR-asymptotic expressions for the secrecy IP are derived.

The PLS analysis is based on the secrecy capacity metric, which is the maximal achievable transmission rate satisfying a certain equivocation rate at the undesired receiver [37]. Mathematically, it is defined as the difference between the legitimate and illegitimate links' capacities as follows

$$C_s = C_l - C_e, \quad (31)$$

where

$$C_l = \log_2(1 + \min(\gamma_{SR}, \gamma_{RD})), \quad (32)$$

and

$$C_e = \log_2(1 + \gamma_{RE}), \quad (33)$$

are the legitimate and eavesdropper's channels capacities, respectively.

To this end, the IP metric represents the probability of the event when the eavesdropper's channel capacity is above the legitimate's, which can be written as [38, Eq. (24)]

$$\begin{aligned} P_{int} &\triangleq \Pr[C_s < 0] \\ &= 1 - \Pr[\min(\gamma_{SR}, \gamma_{RD}) \geq \gamma_{RE}]. \end{aligned} \quad (34)$$

Remark 3. *The overall secrecy capacity in (31) can be expressed as*

$$C_s = \min(C_{SR}, C_{RD}), \quad (35)$$

where

$$C_{UV} = \log_2 \left(\frac{1 + \gamma_{UV}}{1 + \gamma_{RE}} \right), UV \in \{SR, RD\}. \quad (36)$$

- 1) As pointed out in Remark 1.1, the average legitimate SNR per hop, i.e., $\mathbb{E}[\gamma_{UV}]$, is an increasing function of n_{b_i} , while the eavesdropper's average SINR ($\mathbb{E}[\gamma_{RE}]$) is independent of it, as shown in Remark 2. Thus, the higher n_{b_i} , the greater the SNR per-hop, leading to an improved per-hop (eq. (36)) and e2e (eq. (35)) secrecy capacities. As a consequence, the system's IP, given by (eq. (34)), decreases, i.e., better system secrecy.
- 2) Furthermore, $\mathbb{E}[\gamma_{UV}]$ scales with M^2 and N^2 for the S-R and R-D hops, respectively, as discussed in Remark 1.2, while $\mathbb{E}[\gamma_{RE}]$ scales with N in an inadequate scenario for the legitimate nodes (i.e., absence of jamming). Therefore, the ratio of $\mathbb{E}[\gamma_{UV}]$ and $\mathbb{E}[\gamma_{RE}]$ is expressed as

$$\frac{\mathbb{E}[\gamma_{UV}]}{\mathbb{E}[\gamma_{RE}]} = \frac{\mathcal{K}^2 \bar{\gamma}_{UV} 2^{2n_{b_i}} \sin^2 \left(\frac{\pi}{2^{n_{b_i}}} \right)}{16N\bar{\gamma}_{RE}}, \quad (37)$$

with $\mathcal{K} = \begin{cases} M, & \text{if } UV = SR \\ N, & \text{if } UV = RD \end{cases}$. From another front, we have the following function

$$h(y) = y^2 \sin^2 \left(\frac{\pi}{y} \right), \quad (38)$$

where $y = 2^{n_{b_i}} \in [2, \infty[$, and the derivative of $h(y)$ is

$$h'(y) = 2y \sin \left(\frac{\pi}{y} \right) \left[\sin \left(\frac{\pi}{y} \right) - \frac{\pi}{y} \cos \left(\frac{\pi}{y} \right) \right]. \quad (39)$$

Obviously, the sign of $h'(y)$ is the one of $\sin \left(\frac{\pi}{y} \right) - \frac{\pi}{y} \cos \left(\frac{\pi}{y} \right)$. Let us solve the inequality

$$\sin \left(\frac{\pi}{y} \right) - \frac{\pi}{y} \cos \left(\frac{\pi}{y} \right) > 0 \Leftrightarrow \tan \left(\frac{\pi}{y} \right) > \frac{\pi}{y}, \quad (40)$$

which holds for $y \in [2, \infty[$ as has been shown in Remark 1.1. Thus, $h'(y) \geq 0$ which yields that $h(y)$ increases with y , and consequently with n_{b_i} . Henceforth, this yields that $\frac{2^{2n_{b_i}} \sin^2 \left(\frac{\pi}{2^{n_{b_i}}} \right)}{16} \geq \frac{1}{4}$ for $n_{b_i} \geq 1$. To this end, when $\bar{\gamma}_{UV} = \bar{\gamma}_{RE}$, we have the following

$$\frac{\mathbb{E}[\gamma_{UV}]}{\mathbb{E}[\gamma_{RE}]} \geq \frac{\mathcal{K}^2}{4N}. \quad (41)$$

Henceforth, (41) shows that raising the number of REs for $\mathcal{K} > 4$ can boost the legitimate-to-wiretap average SNRs ratio. Consequently, the per-hop and e2e secrecy capacities, given by (36) and (35), respectively, increase. As a result, the IP decreases, i.e., enhanced security.

- 3) It can be obviously noted from (10) and (19) that for $M = N$ and $n_{b_1} = n_{b_2}$ (i.e., $m_{SR} = m_{RD}$, $\Omega_{SR} = \Omega_{RD}$), the CCDF of the end-to-end SNR manifests a symmetric behavior with respect to $\bar{\gamma}_{SR}$ and $\bar{\gamma}_{RD}$, i.e., $\left(F_{\gamma_{eq}}^{(c)}(x) \right)_{\bar{\gamma}_{SR}=\alpha, \bar{\gamma}_{RD}=\beta} = \left(F_{\gamma_{eq}}^{(c)}(x) \right)_{\bar{\gamma}_{SR}=\beta, \bar{\gamma}_{RD}=\alpha}$,

Parameter	Value
$\bar{\gamma}_{SR}, \bar{\gamma}_{RD}$	30 dB
n_{b_1}, n_{b_2}	3 bits
$\bar{\gamma}_{RE}$	40 dB
$\bar{\gamma}_{JE}$	10 dB
M, N	32

TABLE II: Simulation parameters' values.

with $\alpha, \beta > 0$. Furthermore, the IP in (34) can be developed as follows

$$\begin{aligned} P_{int} &= 1 - \Pr[\min(\gamma_{SR}, \gamma_{RD}) \geq \gamma_{RE}] \\ &= 1 - \int_0^\infty F_{\gamma_{eq}}^{(c)}(x) f_{\gamma_{RE}}(x) dx, \end{aligned} \quad (42)$$

which exhibits as well a symmetric behavior with respect to $\bar{\gamma}_{SR}$ and $\bar{\gamma}_{RD}$.

A. Exact Analysis

Proposition 1. The IP of the considered dual-hop RIS-aided WCS can be written in terms of the approximate form given by (43) at the top of the next page, where $H_{p_1, q_1; p_2, p_2; p_3, q_3}^{m_1, n_1; m_2, n_2; m_3, n_3}(\cdot, \cdot | \cdot)$ is the bivariate Fox's H-function [39, Eq. (10.1)], and $\Lambda_i(k, l)$ ($i = 1, 2$) are given by (44) and (45).

Proof: The proof is provided in Appendix B. ■

B. Asymptotic Analysis

Proposition 2. At the high SNR regime ($\bar{\gamma}_{SR} = \bar{\gamma}_{RD} = \bar{\gamma} \rightarrow \infty$), the IP of the considered dual-hop RIS-assisted WCS can be asymptotically expanded as

$$P_{int}^{(\infty)} \sim G_c \bar{\gamma}^{-G_d}, \quad (46)$$

where G_c is defined in (47) shown at the top of the next page, while

$$G_d = \min(m_{SR}, m_{RD}). \quad (48)$$

Proof: The proof is provided in Appendix C. ■

Remark 4. Leveraging (11), it can be noted that the secrecy diversity order, given by (48), is directly proportional to the minimum among the number of REs of $L^{(1)}$ and $L^{(2)}$.

V. NUMERICAL RESULTS

In this section, we provide numerical results for the secrecy level of the analyzed dual-hop RIS-assisted WCS. The system parameters' default values are specified in Table II. Furthermore, throughout the simulation results, the notation $\bar{\gamma}$ is used when the IP is plotted vs $\bar{\gamma}_{SR}$ with $\bar{\gamma}_{RD} = \bar{\gamma}_{SR} = \bar{\gamma}$. Furthermore, we generated 3×10^6 random values for the per-hop fading coefficients, i.e. $h_{SL^{(1)}}$, $h_{L^{(1)R}}$, $h_{RL^{(2)}}$, $h_{JL^{(2)}}$, $h_{L^{(2)D}}$, $h_{L^{(2)E}}$, in order to perform Monte Carlo simulations. Lastly, the simulation results shown in the two-dimensions figures (Except Fig. 8) are represented by x-shaped markers, while analytical results are illustrated by solid lines with different geometric shapes.

In Fig. 2, the IP of the considered dual-hop WCS is shown versus $\bar{\gamma}$. One can remark that the solid lines, corresponding

$$P_{int} \approx 1 - \frac{1}{\Gamma(m_{SR})\Gamma(m_{RD})} \sum_{l=0}^{\infty} \left(\frac{-1}{N\bar{\gamma}_{JE}} \right)^l \left[\sum_{k=1}^2 \frac{1}{l(N\bar{\gamma}_{JE})^{2-k}} H_{2,0;1,2;1,2}^{0,2;2,0;2,0} \left(\frac{m_{SR}\bar{\gamma}_{RE}}{\Omega_{SR}\bar{\gamma}_{SR}\bar{\gamma}_{JE}}, \frac{m_{RD}\bar{\gamma}_{RE}}{\Omega_{RD}\bar{\gamma}_{RD}\bar{\gamma}_{JE}} \mid \Lambda_1(k,l) \right) + \frac{1}{N\bar{\gamma}_{JE}} \sum_{k=1}^2 (1+l)^{k-1} H_{1,0;1,2;1,2}^{0,1;2,0;2,0} \left(\frac{Nm_{SR}\bar{\gamma}_{RE}}{\Omega_{SR}\bar{\gamma}_{SR}}, \frac{Nm_{RD}\bar{\gamma}_{RE}}{\Omega_{RD}\bar{\gamma}_{RD}} \mid \Lambda_2(k,l) \right) \right]. \quad (43)$$

$$\Lambda_1(k,l) = \left((2-k+l, -1, -1), (-l, 1, 1); - : -; (1, 1) : -; (1, 1) \right). \quad (44)$$

$$\Lambda_2(k,l) = \left((k+l, 1, 1); - : -; (1, 1) : -; (1, 1) \right). \quad (45)$$

$$G_c = \begin{cases} \frac{\left(\frac{m_{SR}\bar{\gamma}_{RE}}{\Omega_{SR}\bar{\gamma}_{SR}}\right)^{m_{SR}} \Gamma\left(1-m_{SR}, \frac{1}{N\bar{\gamma}_{JE}}\right)}{\exp\left(-\frac{1}{N\bar{\gamma}_{JE}}\right)}; & M < N \\ \frac{\left(\frac{m_{RD}\bar{\gamma}_{RE}}{\Omega_{RD}\bar{\gamma}_{RD}}\right)^{m_{RD}} \Gamma\left(1-m_{RD}, \frac{1}{N\bar{\gamma}_{JE}}\right)}{\exp\left(-\frac{1}{N\bar{\gamma}_{JE}}\right)}; & M > N \\ \frac{\left(\frac{m_{SR}\bar{\gamma}_{RE}}{\Omega_{SR}\bar{\gamma}_{SR}}\right)^{m_{SR}} \Gamma\left(1-m_{SR}, \frac{1}{N\bar{\gamma}_{JE}}\right)}{\exp\left(-\frac{1}{N\bar{\gamma}_{JE}}\right)} + \frac{\left(\frac{m_{RD}\bar{\gamma}_{RE}}{\Omega_{RD}\bar{\gamma}_{RD}}\right)^{m_{RD}} \Gamma\left(1-m_{RD}, \frac{1}{N\bar{\gamma}_{JE}}\right)}{\exp\left(-\frac{1}{N\bar{\gamma}_{JE}}\right)}; & M = N \end{cases}. \quad (47)$$

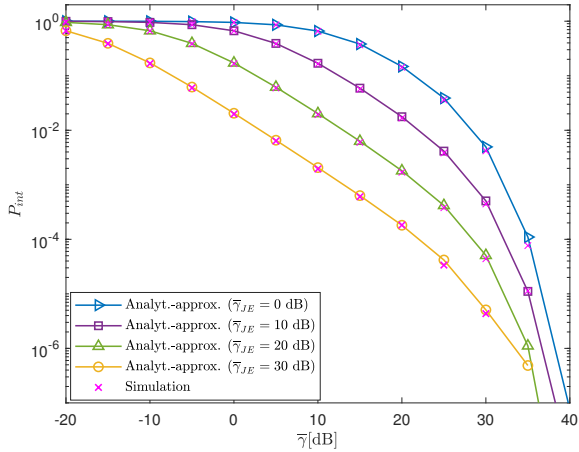


Fig. 2: IP versus $\bar{\gamma}$ for various $\bar{\gamma}_{JE}$ values.

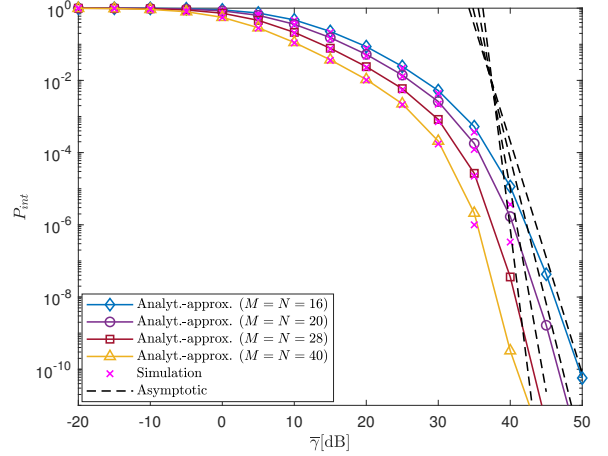


Fig. 3: IP versus $\bar{\gamma}$ for various (M, N) values.

to the derived approximate form in (43), tightly match the simulation results, particularly for $\bar{\gamma} \leq 30$ dB. Furthermore, the IP exhibits a remarkable decrease vs. $\bar{\gamma}$ as expected. Finally, one can ascertain that the higher the jamming power-to-noise ratio, the better the secrecy is, where an IP of 10^{-6} can be reached with $\bar{\gamma}_{JE} = 20$ dB, though the legitimate average SNRs are below the eavesdropper's one.

In Fig. 3, the IP is plotted vs $\bar{\gamma}$ for various values of REs' number (M, N) . Obviously, the system's secrecy improves by increasing the number of REs, as pointed out in *Remarks 1.2* and *3.2*, where one can attain an IP of 10^{-4} with 40 REs for $\bar{\gamma}_{JE} = 10$ dB even when the eavesdropper's link SNR exceeds the legitimate's ones by almost 10 dB (i.e., $\bar{\gamma} = 30$ dB, $\bar{\gamma}_{RE} = 40$ dB). Also, the IP drops to 10^{-6}

with $M, N \geq 28$ while $\bar{\gamma} < \bar{\gamma}_{RE}$. Besides, it is noted that the high-SNR asymptotic dashed curves, plotted from (46), match tightly the approximate's solid-line curves at high SNR values, corroborating the accuracy of the asymptotic analysis.

The influence of the number of quantization bits (i.e., n_{b_1}, n_{b_2}) is shown in Fig. 4, where the IP is plotted with respect to $\bar{\gamma}$ for various n_{b_1} and n_{b_2} values for $\bar{\gamma}_{JE} = 0$ dB. One can ascertain that a very low phase resolution, i.e., $n_{b_1} = n_{b_2} = 1$ bit, yields a remarkable IP degradation. Furthermore, the increase in n_{b_l} ($l = 1, 2$) to 2 bits produces a 5-dB secrecy gain at the high SNR, which endorses the insights discussed in *Remarks 1.1* and *3.1*. Importantly, we ascertain that the secrecy of the system is not improved further when n_{b_l} exceeds 3 bits.

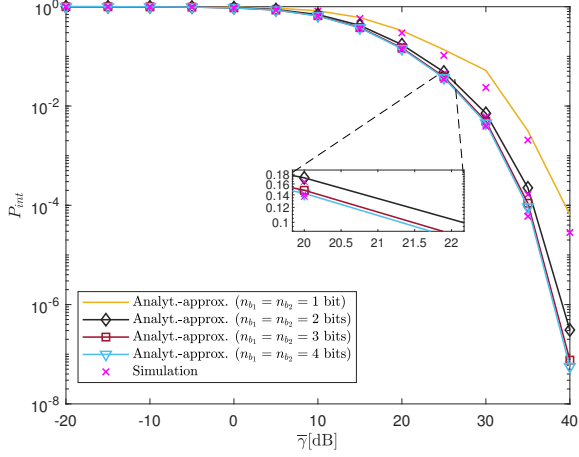


Fig. 4: IP versus $\bar{\gamma}$ for various (n_{b_1}, n_{b_2}) values.

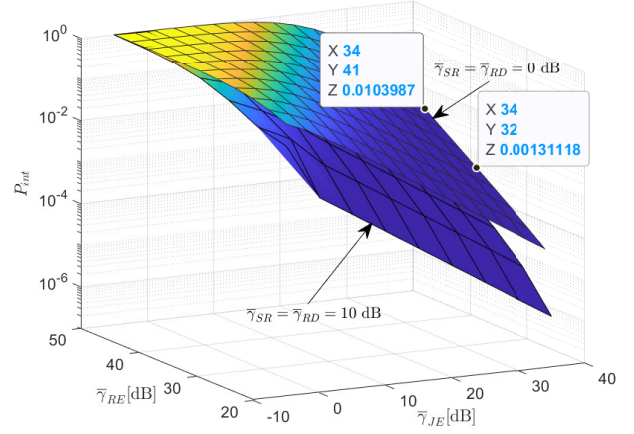


Fig. 6: IP versus $\bar{\gamma}_{RE}$ and $\bar{\gamma}_{JE}$.

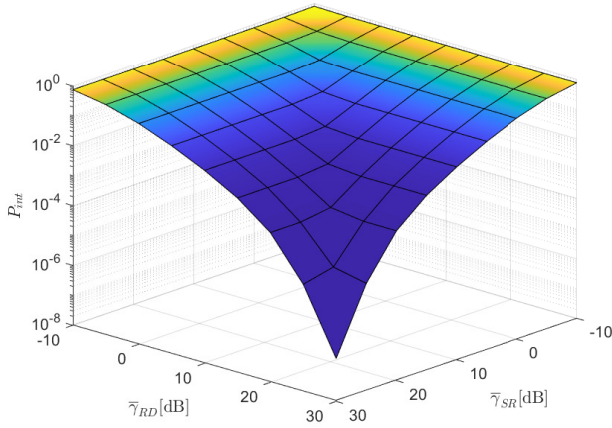


Fig. 5: IP versus $\bar{\gamma}_{SR}$ and $\bar{\gamma}_{RD}$.

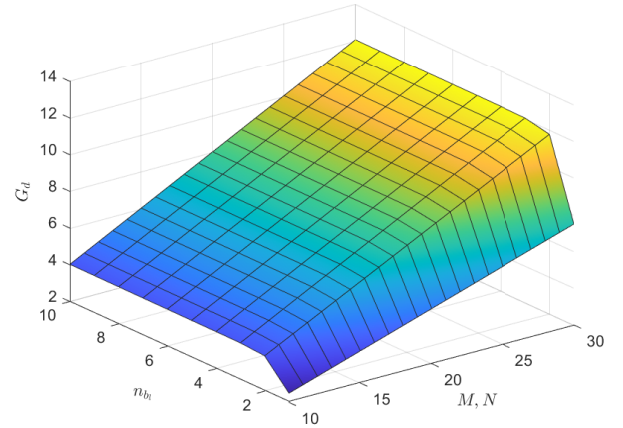


Fig. 7: Secrecy diversity order (G_d) versus (M, N) and n_{b_1} .

The IP is shown in Fig. 5 in three dimensions as a function of both legitimate average SNRs ($\bar{\gamma}_{SR}$ and $\bar{\gamma}_{RD}$), where $\bar{\gamma}_{RE} = 30$ dB and $M = N = 24$. As manifested in the previous figures, the IP decreases when both SNRs increase. Additionally, the IP exhibits a symmetric behavior for both average SNRs, as discussed in Remark 3.3. Furthermore, it is worth noting that when $\bar{\gamma}_{SR}$ ($\bar{\gamma}_{RD}$) is fixed, the IP reveals horizontal floors at high $\bar{\gamma}_{RD}$ ($\bar{\gamma}_{SR}$). In fact, the e2e SNR γ_{eq} , given by (18), equals the minimum among γ_{SR} and γ_{RD} . To this end, the IP reaches the saturation regime at high $\bar{\gamma}_{SR}$ ($\bar{\gamma}_{RD}$) values when $\bar{\gamma}_{RD}$ ($\bar{\gamma}_{SR}$) is fixed.

Fig. 6 presents the IP behavior versus $\bar{\gamma}_{RE}$ and $\bar{\gamma}_{JE}$, where $\bar{\gamma}_{SR} = \bar{\gamma}_{RD} = 0, 10$ dB. Expectedly, the system's security level deteriorates when $\bar{\gamma}_{RE}$ increases, i.e., 100% IP is manifested for $\bar{\gamma}_{SR} = \bar{\gamma}_{RD} = 0$ dB, $\bar{\gamma}_{JE} \leq 0$ dB and $\bar{\gamma}_{RE} \geq 40$ dB. Importantly, jamming can effectively improve the security where the IP can be maintained around 10^{-2} and 1.3×10^{-3} , for $\bar{\gamma}_{JE} = 34$ dB, even when the SNR of the illegitimate channel is 41 and 32 dB-advantageous over the legitimate links', respectively.

The system's secrecy diversity order is illustrated in Fig. 7 in terms of the number of REs (M, N) and n_{b_1} . As discussed in Remark 4, the system's diversity order increases with the increase in the number of REs. That is, the higher the number of REs, the greater the IP slope at high SNR as can be noted as well from the asymptotic curves in Fig. 3. Also, the diversity order is less impacted by n_{b_1} above 2 bits.

In Fig. 8, a comparative IP analysis is provided between the considered system and two distinct setups of single-RIS dual-hop WCSs, namely: when the RIS is incorporated only in the first hop (*Setup I*) or the second hop (*Setup II*). It is worthy to mention that the results for *Setups I* and *II* were obtained by virtue of Monte Carlo simulations. Also, we set $M = N$. The results show that the analyzed system clearly outperforms the aforementioned schemes in terms of PLS. Furthermore, we observe that *Setup I*, i.e., RIS incorporated only in the first hop, exhibits a slight secrecy improvement compared to *Setup II*, i.e., RIS in the second hop, where the eavesdropper and legitimate destination in the latter case benefit from the SNR improvement through involving the RIS in the second

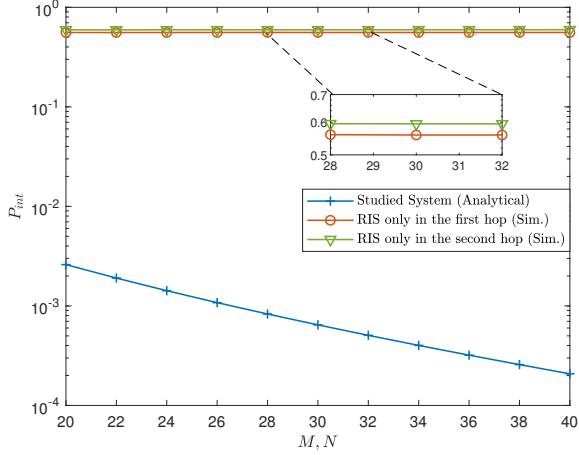


Fig. 8: IP versus $\bar{\gamma}_{SR}$: A comparative analysis with single-RIS dual-hop systems.

hop. Furthermore, it is obvious that the analyzed system's IP manifests a decreasing behavior vs (M, N) , different from *Setups I* and *II*, where the IP is constant with respect to the number of REs. This is due to the saturation effect of the DF relaying's e2e SNR, given by (18), where γ_{eq} equals γ_{RD} regardless of boosting γ_{SR} by increasing the number of REs (*Setup I*) or vice-versa (*Setup II*).

VI. CONCLUSION

In this paper, we provide a thorough analysis of the secrecy performance of a dual-hop RIS-assisted and jamming-aided WCS. The setup consists of a source transmitting information signals to a destination through a DF relay. Two RISs assist the source-relay and relay-destination communications. We assume the presence of an eavesdropper that attempts to overhear the signal forwarded by the relay and reflected by the second RIS. We also introduce a friendly jammer to increase the security level by means of a broadcasted jamming signal. Finally, we assume that RISs phase shifts are subject to PQEs.

Tight approximate and asymptotic IP expressions were derived, where the impact of key system parameters was discussed. Our results showed that the system's IP is significantly improved by increasing the jamming power and number of REs, where the IP can reach 10^{-6} with 40 REs and 10 dB of jamming power-to-noise ratio, even when the legitimate average SNRs are below the wiretap one. Furthermore, we showed that there is no impact on the secrecy of the system when the number of quantization bits exceeds 3 bits. Importantly, the results also illustrate the efficiency of jamming in maintaining lower IP levels in strong eavesdropping scenarios (i.e., the eavesdropper's SNR is much higher compared to the legitimate one) with a fixed number of REs. We showed as well that the secrecy diversity order is proportional to the minimum among both RISs' number of REs. Lastly, the analyzed system shows remarkable secrecy improvement compared to the single-RIS dual-hop networks, i.e., RIS involved in one of the two hops.

ACKNOWLEDGMENT

This research was sponsored in part by the NATO Science for Peace and Security Programme under grant SPS G5797.

APPENDIX A: PROOF OF LEMMA 1

First, let us compute the correlation coefficient between g_{RE} and g_{JE} , given by (29) and (30), respectively, as follows

$$\rho_1 = \frac{\mathbb{E}[g_{RE}g_{JE}] - \mu_{g_{RE}}\mu_{g_{JE}}}{\sqrt{\sigma_{g_{RE}}\sigma_{g_{JE}}}}, \quad (49)$$

where

$$\mu_{g_{XY}} = \mathbb{E}[g_{XY}], \quad (50)$$

$$\sigma_{g_{XY}} = \mathbb{E}[g_{XY}^2] - \mu_{g_{XY}}^2. \quad (51)$$

with $XY \in \{RD, RE, JE\}$. Leveraging (i) the linearity of the expectation operator along with (ii) $\mathbb{E}[h_{AB}] = 0$ ($A, B \in \{R, D, J, E, (L_k^{(2)})_{1 \leq k \leq N}\}$) for complex Gaussian distribution (i.e., Rayleigh fading channels) and (iii) (4), (5), (9), (29), and (30), one can find that $\mu_{g_{JE}} = \mu_{g_{RE}} = 0$ regardless of the distributions of η_i and ϖ_i . Thus, (49) reduces to

$$\rho_1 = \frac{\mathbb{E}[g_{RE}g_{JE}]}{\sqrt{\sigma_{g_{RE}}\sigma_{g_{JE}}}}. \quad (52)$$

By plugging (29) and (30) into (52), its numerator can be written as

$$\begin{aligned} \mathbb{E}[g_{RE}g_{JE}] &= \sum_{i=1}^N \sum_{k=1}^N \mathbb{E} \left[\left| h_{RL_i^{(2)}} \right| e^{j \left\{ \xi_i^{(2)} - \arg \left(h_{L_i^{(2)D}} \right) \right\}} \right] \\ &\quad \times \underbrace{\mathbb{E} \left[h_{JL_k^{(2)}} \right] \mathbb{E} \left[h_{L_k^{(2)E}} h_{L_k^{(2)D}} \right]}_{=0} \\ &\quad \times \mathbb{E} \left[e^{j \left\{ -\arg \left(h_{RL_k^{(2)}} \right) - \arg \left(h_{L_k^{(2)D}} \right) + \xi_k^{(2)} \right\}} \right], \end{aligned} \quad (53)$$

which vanishes to 0. Therefore, g_{RE} and g_{JE} are uncorrelated. By following a similar rationale for the correlations between (g_{RD} and g_{RE}) and (g_{RD} and g_{JE}), one can find that the respective correlation coefficients are sums of products involving the expectation of $h_{L_k^{(2)E}}$ multiplied by the average of the remaining involved links' fading envelopes, phase shifts, and PQEs. Thus, as $\mathbb{E}[h_{AB}] = 0$, both correlation coefficients vanish, resulting in the mutual independence of g_{RD} , g_{RE} , and g_{JE} . This concludes the proof of *Lemma 1*.

APPENDIX B: PROOF OF PROPOSITION 1

From the IP definition in (34), we can express it as follows

$$P_{int} = 1 - \int_0^\infty F_{\gamma_{eq}}^{(c)}(x) f_{\gamma_{RE}}(x) dx. \quad (54)$$

Thus, we attain (55) shown at the top of the next page, where *Step (a)* is obtained by involving the CCDF and PDF expressions from (19) and (26) into (54) along with using [40, Eq. (06.06.26.0005.01)], while *Step (b)* is produced via

$$\begin{aligned}
P_{int} &\stackrel{(a)}{\approx} 1 - \frac{1}{N\Gamma(m_{SR})\Gamma(m_{RD})} \int_0^\infty G_{1,2}^{2,0} \left(\frac{m_{SR}}{\Omega_{SR}\bar{\gamma}_{SR}} x \middle| \begin{matrix} -; 1 \\ 0, m_{SR} \end{matrix} \right) G_{1,2}^{2,0} \left(\frac{m_{RD}}{\Omega_{RD}\bar{\gamma}_{RD}} x \middle| \begin{matrix} -; 1 \\ 0, m_{RD} \end{matrix} \right) \\
&\quad \times \frac{\exp\left(-\frac{x}{N\bar{\gamma}_{RE}}\right) [\bar{\gamma}_{JE}N\bar{\gamma}_{RE} + \bar{\gamma}_{RE} + \bar{\gamma}_{JE}x]}{(\bar{\gamma}_{RE} + \bar{\gamma}_{JE}x)^2} dx, \\
&\stackrel{(b)}{=} 1 - \frac{1}{(2\pi j)^2 N\Gamma(m_{SR})\Gamma(m_{RD})} \int_{C_s} \int_{C_v} \frac{\Gamma(s)\Gamma(m_{SR}+s)\Gamma(v)\Gamma(m_{RD}+v)}{\Gamma(1+s)\Gamma(1+v)} \int_0^\infty [\bar{\gamma}_{JE}(N\bar{\gamma}_{RE}+x) + \bar{\gamma}_{RE}] \\
&\quad \times \underbrace{\frac{\exp\left(-\frac{x}{N\bar{\gamma}_{RE}}\right)}{(\bar{\gamma}_{RE} + \bar{\gamma}_{JE}x)^2} x^{-s-v} dx}_{\triangleq F(s,v)=F_1(s,v)+F_2(s,v)} \left(\frac{m_{SR}}{\Omega_{SR}\bar{\gamma}_{SR}}\right)^{-s} \left(\frac{m_{RD}}{\Omega_{RD}\bar{\gamma}_{RD}}\right)^{-v} dsdv, \tag{55}
\end{aligned}$$

$$\begin{aligned}
P_{int} &\approx 1 - \frac{1}{(2\pi j)^3 \Gamma(m_{SR})\Gamma(m_{RD})} \sum_{i=1}^2 (\bar{\gamma}_{JE}N)^{i-2} \int_{C_s} \int_{C_v} \int_{C_w} \frac{\Gamma(s)\Gamma(m_{SR}+s)\Gamma(v)\Gamma(m_{RD}+v)}{\Gamma(1+s)\Gamma(1+v)} \\
&\quad \times \Gamma(w)\Gamma(1-s-v-w)\Gamma(i-1+s+v+w) \left(\frac{m_{SR}}{\Omega_{SR}\bar{\gamma}_{SR}} \frac{\bar{\gamma}_{RE}}{\bar{\gamma}_{JE}}\right)^{-s} \left(\frac{m_{RD}}{\Omega_{RD}\bar{\gamma}_{RD}} \frac{\bar{\gamma}_{RE}}{\bar{\gamma}_{JE}}\right)^{-v} \left(\frac{1}{N\bar{\gamma}_{JE}}\right)^{-w} dsdvdw. \tag{57}
\end{aligned}$$

the Mellin-Barnes integral (MBI) definition [41, Eq. (1.112)] with

$$\begin{aligned}
\mathcal{F}_i(s,v) &\triangleq (\bar{\gamma}_{JE}N\bar{\gamma}_{RE})^{i-1} \int_0^\infty \frac{\exp\left(-\frac{x}{N\bar{\gamma}_{RE}}\right)}{(\bar{\gamma}_{RE} + \bar{\gamma}_{JE}x)^i} x^{-s-v} dx. \\
&\stackrel{(a)}{=} (\bar{\gamma}_{JE}N\bar{\gamma}_{RE})^{i-1} \int_0^\infty \frac{x^{-s-v}}{(\bar{\gamma}_{RE} + \bar{\gamma}_{JE}x)^i} \\
&\quad \times G_{0,1}^{1,0} \left(\frac{x}{N\bar{\gamma}_{RE}} \middle| \begin{matrix} -; - \\ 0; - \end{matrix} \right) dx, \\
&\stackrel{(b)}{=} \frac{(\bar{\gamma}_{JE}N\bar{\gamma}_{RE})^{i-1}}{2\pi j} \int_{C_w} \Gamma(w) \left(\frac{1}{N\bar{\gamma}_{RE}}\right)^{-w} \\
&\quad \times \int_0^\infty \frac{x^{-s-v-w}}{(\bar{\gamma}_{RE} + \bar{\gamma}_{JE}x)^i} dx dw, \\
&\stackrel{(c)}{=} \frac{\bar{\gamma}_{JE}^{i-2} N^{i-1}}{2\pi j} \int_{C_w} \Gamma(w) \left(\frac{1}{N\bar{\gamma}_{JE}}\right)^{-w} \left(\frac{\bar{\gamma}_{RE}}{\bar{\gamma}_{JE}}\right)^{-s} \\
&\quad \times \Gamma(1-s-v-w)\Gamma(i-1+s+v+w) dw. \tag{56}
\end{aligned}$$

Step (a) of (56) yields by means of [40, Eq. (07.34.03.0228.01)], while using [41, Eq. (1.112)] produces *Step (b)*. Finally, leveraging [34, Eqs. (3.194.3, 8.384.1)] , *Step (c)* holds.

By plugging (56) into (55), it yields (57) at the top of the page.

Importantly, armed by the residues theorem, such a triple MBI can be reduced to a double MBI by evaluating the series of residues on the left half-plane poles of both $\Gamma(w)$ and $\Gamma(i-1+s+v+w)$ as shown in (58) at the top of the next page [42, Theorem 1.2]

Finally, relying on the bivariate Fox's H -function definition in [39, Eqs. (1.11-1.13)] along with some algebraic manipula-

tions and simplifications, (43) is reached. This concludes the proposition's proof.

APPENDIX C: PROOF OF PROPOSITION 2

At the high SNR regime ($\bar{\gamma}_{SR} = \bar{\gamma}_{RD} = \bar{\gamma} \rightarrow \infty$), the IP can be expanded as follows

$$P_{int}^{(\infty)} \sim 1 - \int_0^\infty F_{\gamma_{eq}}^{(c,\infty)}(x) f_{\gamma_{RE}}(x) dx \tag{59}$$

$$\begin{aligned}
&\stackrel{(a)}{=} 1 - \frac{1}{N} \int_0^\infty \frac{[\bar{\gamma}_{JE}N\bar{\gamma}_{RE} + \bar{\gamma}_{RE} + \bar{\gamma}_{JE}x]}{(\bar{\gamma}_{RE} + \bar{\gamma}_{JE}x)^2} \\
&\quad \times \exp\left(-\frac{x}{N\bar{\gamma}_{RE}}\right) \frac{\left(\Gamma(m_{SR}) - \frac{(\frac{m_{SR}}{\Omega_{SR}\bar{\gamma}_{SR}}x)^{m_{SR}}}{m_{SR}}\right)}{\Gamma(m_{SR})} \\
&\quad \times \frac{\left(\Gamma(m_{RD}) - \frac{(\frac{m_{RD}}{\Omega_{RD}\bar{\gamma}_{RD}}x)^{m_{RD}}}{m_{RD}}\right)}{\Gamma(m_{RD})} dx \tag{60}
\end{aligned}$$

$$\stackrel{(b)}{=} \mathcal{G}_1 + \mathcal{G}_2 - \mathcal{G}_3, \tag{61}$$

with $(\mathcal{G}_i)_{1 \leq i \leq 3}$ are given by (62)-(64) in the next page, where *Step (a)* in (60) is reached by incorporating the CCDF of γ_{eq} in (19) and the PDF of γ_{RE} in (26) into (59) along with the upper incomplete Gamma expansion [40, Eq. (06.06.06.0001.02)], while *Step (b)* yields by expanding *Step (a)* and taking into account that $\int_0^\infty f_{\gamma_{RE}}(x) dx = 1$.

Importantly, one can note that the IP expression in (61) is the sum of three terms, given by (62)-(64), where each of which has a different coding gain and diversity order pair. Thus, the IP will be expanded by the term having the lowest power of $\bar{\gamma}$. Henceforth, three different cases are distinguished, namely:

$$P_{int} \approx 1 - \frac{1}{\Gamma(m_{SR})\Gamma(m_{RD})(2\pi j)^2} \sum_{l=0}^{\infty} \frac{(-1)^l}{l!} \sum_{i=1}^2 (\bar{\gamma}_{JE}N)^{i-2} \int_{C_s} \int_{C_v} \frac{\Gamma(s)\Gamma(m_{SR}+s)\Gamma(v)\Gamma(m_{RD}+v)}{\Gamma(1+s)\Gamma(1+v)} \times \left(\frac{m_{SR}}{\Omega_{SR}\bar{\gamma}_{SR}} \frac{\bar{\gamma}_{RE}}{\bar{\gamma}_{JE}} \right)^{-s} \left(\frac{m_{RD}}{\Omega_{RD}\bar{\gamma}_{RD}} \frac{\bar{\gamma}_{RE}}{\bar{\gamma}_{JE}} \right)^{-v} \left[\frac{\Gamma(1-s-v+l)\Gamma(i-1+s+v-l)}{\Gamma(-s-v-l-i+1)\Gamma(l+i)} + \frac{(N\bar{\gamma}_{JE})^l}{(N\bar{\gamma}_{JE})^{s+v+l+i-1}} \right] dsdv. \quad (58)$$

$$\mathcal{G}_1 = \frac{\bar{\gamma}^{-m_{SR}}}{\Gamma(m_{SR})} \int_0^{\infty} \frac{\left(\frac{m_{SR}}{\Omega_{SR}}x\right)^{m_{SR}} \exp\left(-\frac{x}{N\bar{\gamma}_{RE}}\right) [\bar{\gamma}_{JE}N\bar{\gamma}_{RE} + \bar{\gamma}_{RE} + \bar{\gamma}_{JE}x]}{m_{SR} N(\bar{\gamma}_{RE} + \bar{\gamma}_{JE}x)^2} dx. \quad (62)$$

$$\mathcal{G}_2 = \frac{\bar{\gamma}^{-m_{RD}}}{\Gamma(m_{RD})} \int_0^{\infty} \frac{\left(\frac{m_{RD}}{\Omega_{RD}}x\right)^{m_{RD}} \exp\left(-\frac{x}{N\bar{\gamma}_{RE}}\right) [\bar{\gamma}_{JE}N\bar{\gamma}_{RE} + \bar{\gamma}_{RE} + \bar{\gamma}_{JE}x]}{m_{RD} N(\bar{\gamma}_{RE} + \bar{\gamma}_{JE}x)^2} dx. \quad (63)$$

$$\mathcal{G}_3 = \frac{\bar{\gamma}^{-(m_{SR}+m_{RD})}}{\Gamma(m_{SR})\Gamma(m_{RD})} \int_0^{\infty} \frac{\left(\frac{m_{SR}}{\Omega_{SR}}x\right)^{m_{SR}} \left(\frac{m_{RD}}{\Omega_{RD}}x\right)^{m_{RD}} \exp\left(-\frac{x}{N\bar{\gamma}_{RE}}\right) [\bar{\gamma}_{JE}N\bar{\gamma}_{RE} + \bar{\gamma}_{RE} + \bar{\gamma}_{JE}x]}{m_{SR} m_{RD} N(\bar{\gamma}_{RE} + \bar{\gamma}_{JE}x)^2} dx. \quad (64)$$

$$\begin{aligned} \mathcal{G}_1 &\stackrel{(a)}{=} \bar{\gamma}^{-m_{SR}} \frac{\left(\frac{m_{SR}}{\Omega_{SR}}\right)^{m_{SR}}}{N\Gamma(m_{SR}+1)} \underbrace{\left[\frac{1}{\bar{\gamma}_{JE}} \int_0^{\infty} x^{m_{SR}} \frac{\exp\left(-\frac{x}{N\bar{\gamma}_{RE}}\right)}{\frac{\bar{\gamma}_{RE}}{\bar{\gamma}_{JE}} + x} dx + \bar{\gamma}_{JE}N\bar{\gamma}_{RE} \int_0^{\infty} x^{m_{SR}} \frac{\exp\left(-\frac{x}{N\bar{\gamma}_{RE}}\right)}{(\bar{\gamma}_{RE} + \bar{\gamma}_{JE}x)^2} dx \right]}_{\triangleq G_c} \\ &\stackrel{(b)}{=} \bar{\gamma}^{-m_{SR}} \frac{\left(\frac{m_{SR}}{\Omega_{SR}}\right)^{m_{SR}}}{N\Gamma(m_{SR}+1)} \left[\frac{1}{\bar{\gamma}_{JE}} \int_0^{\infty} x^{m_{SR}} \frac{\exp\left(-\frac{x}{N\bar{\gamma}_{RE}}\right)}{\frac{\bar{\gamma}_{RE}}{\bar{\gamma}_{JE}} + x} dx - N\bar{\gamma}_{RE} \underbrace{\left[\frac{x^{m_{SR}} \exp\left(-\frac{x}{N\bar{\gamma}_{RE}}\right)}{\bar{\gamma}_{RE} + \bar{\gamma}_{JE}x} \right]_0^{\infty}}_{=0} \right. \\ &\quad \left. + N\bar{\gamma}_{RE} \int_0^{\infty} \frac{[m_{SR}x^{m_{SR}-1} \exp\left(-\frac{x}{N\bar{\gamma}_{RE}}\right) - \frac{1}{N\bar{\gamma}_{RE}} x^{m_{SR}} \exp\left(-\frac{x}{N\bar{\gamma}_{RE}}\right)]}{\bar{\gamma}_{RE} + \bar{\gamma}_{JE}x} dx \right]. \quad (65) \end{aligned}$$

A. Case I: $M < N$

Since m_{SR} and m_{RD} are proportional to M and N , respectively, the IP will be expanded by \mathcal{G}_1 in (62) for which the diversity order equals m_{SR} . Henceforth, it yields (65) at the top of the page, where *Step (a)* holds by decomposing (62) into two terms, while *Step (b)* is reached via the use of integration by parts with $f'(x) = (\bar{\gamma}_{RE} + \bar{\gamma}_{JE}x)^{-2}$ and $g(x) = x^{m_{SR}} \exp\left(-\frac{x}{N\bar{\gamma}_{RE}}\right)$. Finally, by utilizing [34, Eq. (3.383.10)] along with some algebraic manipulations, the first case of (47) is attained.

B. Case II: $M > N$

In this case, the IP will be expanded by \mathcal{G}_2 . By following a similar rationale to *Case I* and substituting the index SR by RD , we reach the second case of (47).

C. Case III: $M = N$

In this case, the IP is expanded by the sum of the two terms produced in the previous cases, yielding the third case of (47). This concludes the proof of *Proposition 2*.

REFERENCES

- [1] E. Illi, M. K. Qaraqe, F. El Bouanani, and S. M. Al-Kuwari, "On the secrecy analysis of a RIS-aided wireless communication system subject to phase quantization errors," *To appear in the 5th Internat. Balkan Conf. Commun. Netw. (Balkancom 2022) Proc.*, Jul. 2022.
- [2] W. Saad, M. Bennis, and M. Chen, "A vision of 6G wireless systems: Applications, trends, technologies, and open research problems," *IEEE Netw.*, vol. 34, no. 3, pp. 134–142, May/Jun. 2020.
- [3] V.-L. Nguyen, P.-C. Lin, B.-C. Cheng, R.-H. Hwang, and Y.-D. Lin, "Security and privacy for 6G: A survey on prospective technologies and challenges," *IEEE Commun. Surveys Tuts.*, vol. 23, no. 4, pp. 2384–2428, Fourthquarter 2021.
- [4] E. Illi, F. El Bouanani, D. B. da Costa, F. Ayoub, and U. S. Dias, "Dual-hop mixed RF-UOW communication system: A PHY security analysis," *IEEE Access*, vol. 6, pp. 55 345–55 360, 2018.
- [5] N. Xie, Z. Li, and H. Tan, "A survey of physical-layer authentication in wireless communications," *IEEE Commun. Surveys Tuts.*, vol. 23, no. 1, pp. 282–310, Firstquarter 2021.
- [6] J. M. Hamamreh, H. M. Furqan, and H. Arslan, "Classifications and applications of physical layer security techniques for confidentiality: A comprehensive survey," *IEEE Commun. Surveys Tuts.*, vol. 21, no. 2, pp. 1773–1828, Secondquarter 2019.
- [7] C. Feng and H.-M. Wang, "Secure short-packet communications at the physical layer for 5G and beyond," *IEEE Communications Standards Magazine*, vol. 5, no. 3, pp. 96–102, Sep. 2021.
- [8] A. D. Wyner, "The wire-tap channel," *The Bell System Technical Journal*, vol. 54, no. 8, pp. 1355–1387, Oct 1975.
- [9] E. Illi, F. El Bouanani, D. B. da Costa, P. C. Sofotasios, F. Ayoub, K. Mezher, and S. Muhaidat, "Physical layer security of a dual-hop

- regenerative mixed RF/UOW system," *IEEE Trans. Sustain. Comput.*, vol. 6, no. 1, pp. 90–104, Jan.-Mar. 2021.
- [10] O. Özdoğan, E. Björnson, and E. G. Larsson, "Intelligent reflecting surfaces: Physics, propagation, and pathloss modeling," *IEEE Wireless Commun. Lett.*, vol. 9, no. 5, pp. 581–585, May 2020.
- [11] E. Björnson, O. Özdoğan, and E. G. Larsson, "Reconfigurable intelligent surfaces: Three myths and two critical questions," *IEEE Commun. Mag.*, vol. 58, no. 12, pp. 90–96, Jan. 2021.
- [12] C. Pan, H. Ren, K. Wang, W. Xu, M. Elkashlan, A. Nallanathan, and L. Hanzo, "Multicell MIMO communications relying on intelligent reflecting surfaces," *IEEE Trans. Wireless Commun.*, vol. 19, no. 8, pp. 5218–5233, Aug. 2020.
- [13] X. Guan, Q. Wu, and R. Zhang, "Intelligent reflecting surface assisted secrecy communication: Is artificial noise helpful or not?" *IEEE Wireless Commun. Lett.*, vol. 9, no. 6, pp. 778–782, Jun. 2020.
- [14] L. Lv, Q. Wu, Z. Li, N. Al-Dhahir, and J. Chen, "Secure two-way communications via intelligent reflecting surfaces," *IEEE Commun. Lett.*, vol. 25, no. 3, pp. 744–748, Mar. 2021.
- [15] L. Yang, J. Yang, W. Xie, M. O. Hasna, T. Tsiftsis, and M. D. Renzo, "Secrecy performance analysis of RIS-aided wireless communication systems," *IEEE Trans. Veh. Technol.*, vol. 69, no. 10, pp. 12296–12300, Oct. 2020.
- [16] Z. Tang, T. Hou, Y. Liu, J. Zhang, and L. Hanzo, "Physical layer security of intelligent reflective surface aided NOMA networks," *IEEE Trans. Veh. Technol.*, vol. 71, no. 7, Jul. 2022.
- [17] X. Gu, W. Duan, G. Zhang, Q. Sun, M. Wen, and P.-H. Ho, "Physical layer security for RIS-aided wireless communications with uncertain eavesdropper distributions," *IEEE Syst. J.*, pp. 1–12, 2022.
- [18] S. Fang, G. Chen, Z. Abdullah, and Y. Li, "Intelligent omni surface-assisted secure MIMO communication networks with artificial noise," *IEEE Commun. Lett.*, vol. 26, no. 6, Jun. 2022.
- [19] Z. Li, S. Wang, M. Wen, and Y.-C. Wu, "Secure multicast energy-efficiency maximization with massive RISs and uncertain CSI: First-order algorithms and convergence analysis," *IEEE Trans. Wireless Commun.*, pp. 1–1, 2022, early Access.
- [20] T. Cai, J. Zhang, S. Yan, L. Meng, J. Sun, and N. Al-Dhahir, "Reconfigurable intelligent surface aided non-orthogonal unicast-multicast secure transmission," *IEEE Wireless Commun. Lett.*, vol. 11, no. 3, pp. 578–582, Mar. 2022.
- [21] M. H. Khoshafa, T. M. N. Ngatched, and M. H. Ahmed, "Reconfigurable intelligent surfaces-aided physical layer security enhancement in D2D underlay communications," *IEEE Commun. Lett.*, vol. 25, no. 5, pp. 1443–1447, May 2021.
- [22] J. Luo, F. Wang, S. Wang, H. Wang, and D. Wang, "Reconfigurable intelligent surface: Reflection design against passive eavesdropping," *IEEE Trans. Wireless Commun.*, vol. 20, no. 5, pp. 3350–3364, May 2021.
- [23] M.-A. Badiu and J. P. Coon, "Communication through a large reflecting surface with phase errors," *IEEE Wireless Commun. Lett.*, vol. 9, no. 2, pp. 184–188, Feb. 2020.
- [24] J. D. Vega Sánchez, P. Ramírez-Espinosa, and F. J. López-Martínez, "Physical layer security of large reflecting surface aided communications with phase errors," *IEEE Wireless Commun. Lett.*, vol. 10, no. 2, pp. 325–329, Feb. 2021.
- [25] P. Xu, G. Chen, G. Pan, and M. D. Renzo, "Ergodic secrecy rate of RIS-assisted communication systems in the presence of discrete phase shifts and multiple eavesdroppers," *IEEE Wireless Commun. Lett.*, vol. 10, no. 3, pp. 629–633, Mar. 2021.
- [26] I. Trigui, W. Ajib, and W.-P. Zhu, "Secrecy outage probability and average rate of RIS-aided communications using quantized phases," *IEEE Commun. Lett.*, vol. 25, no. 6, pp. 1820–1824, Jun. 2021.
- [27] X. Zhao and J. Sun, "Secure reconfigurable intelligent surface aided heterogeneous VLC-RF cooperative NOMA networks," *Optics Communications*, vol. 511, pp. 1–8, May 2022.
- [28] C. Huang, G. Chen, and K.-K. Wong, "Multi-agent reinforcement learning-based buffer-aided relay selection in IRS-assisted secure cooperative networks," *IEEE Trans. Inf. Forensics Security*, vol. 16, pp. 4101–4112, 2021.
- [29] T. Hossain, S. Shabab, A. S. M. Badrudduza, M. K. Kundu, I. S. Ansari, "On the physical layer security performance over RIS-aided dual-hop RF-UOWC mixed network," *CoRR*, vol. abs/2112.06487, 2021. [Online]. Available: <http://arxiv.org/abs/2112.06487>
- [30] B. Zafar, S. Gherekhloo, and M. Haardt, "Analysis of multihop relaying networks: Communication between range-limited and cooperative nodes," *IEEE Veh. Technol. Mag.*, vol. 7, no. 3, pp. 40–47, Sep. 2012.
- [31] I. Yildirim, F. Kilinc, E. Basar, and G. C. Alexandropoulos, "Hybrid RIS-empowered reflection and decode-and-forward relaying for coverage extension," *IEEE Commun. Lett.*, vol. 25, no. 5, pp. 1692–1696, May 2021.
- [32] W. Guo, H. Zhao, and Y. Tang, "Testbed for cooperative jamming cancellation in physical layer security," *IEEE Wireless Commun. Lett.*, vol. 9, no. 2, pp. 240–243, Feb. 2020.
- [33] E. Björnson, H. Wymeersch, B. Matthiesen, P. Popovski, L. Sanguinetti, and E. de Carvalho, "Reconfigurable intelligent surfaces: A signal processing perspective with wireless applications," *IEEE Signal Process. Mag.*, vol. 39, no. 2, pp. 135–158, Mar. 2022.
- [34] I. S. Gradshteyn and I. M. Ryzhik, *Table of Integrals, Series, and Products: 7th Edition*. Burlington, MA: Elsevier, 2007.
- [35] L. Yang and Y. Yuan, "Secrecy outage probability analysis for RIS-assisted NOMA systems," *Electron. Lett.*, vol. 56, no. 23, p. 1254–1256, Nov. 2020.
- [36] E. Basar, M. Di Renzo, J. De Rosny, M. Debbah, M.-S. Alouini, and R. Zhang, "Wireless communications through reconfigurable intelligent surfaces," *IEEE Access*, vol. 7, pp. 116753–116773, 2019.
- [37] M. Bloch, J. Barros, M. R. D. Rodrigues, and S. W. McLaughlin, "Wireless Information-Theoretic Security," *IEEE Trans. Inf. Theory*, vol. 54, no. 6, pp. 2515–2534, Jun. 2008.
- [38] E. Illi, F. El Bouanani, F. Ayoub, and M.-S. Alouini, "A PHY layer security analysis of a hybrid high throughput satellite with an optical feeder link," *IEEE Open J. Commun. Soc.*, vol. 1, pp. 713–731, 2020.
- [39] N. T. Hai and S. B. Yakubovich, *The Double Mellin-Barnes Type Integrals and their Applications to Convolution Theory*. P O Box 128, Farrer Road, Singapore 9128: World Scientific Publishing Co. Pte. Ltd, 1992.
- [40] I. W. Research, *Mathematica Edition: version 13.1*. Champaign, Illinois: Wolfram Research, Inc., 2022.
- [41] A. Mathai, R. K. Saxena, and H. J. Haubol, *The H-Function Theory and Applications*. New York: Springer, 2010.
- [42] A. A. Kilbas and M. Saigo, *H-Transforms: Theory and Applications*. Boca Raton, Florida, US: CRC Press, 2004.